Fast-Pixel-Matching Algorithm for Automated Shear Stud Welding Based on the Integration of 2D Drawings and Structured Light Cameras

Huiguang Wang[1], Lu Deng[1,2,*], Ran Cao[1,2], and Jingjing Guo[1,2]

[1]College of Civil Engineering, Hunan University, China
[2]Hunan Provincial Key Laboratory for Damage Diagnosis for Engineering Structures, Hunan University, China
[*]Corresponding Author
whg0917@hnu.edu.cn, [*]denglu@hnu.edu.cn, rcao@hnu.edu.cn, guojingjing@hnu.edu.cn

Abstract –

Due to the lack of depth information, using 2D drawings to guide robotic manufacturing is difficult, such as stud welding and drilling. In this paper, a new algorithm, Fast-Pixel-Matching (FPM), is proposed to provide depth information for precise point positioning based on 2D drawings and structured light cameras. Based on our experiment, the efficiency of the FPM process is found to be at least 20 times higher than the brute-force search (BFS) method. Also, we demonstrated that the algorithm can be applied to automated stud welding, where the efficiency of positioning can be significantly improved and the positioning accuracy of the proposed method meets the code requirements.

Keywords –

Point positioning; 2D drawings; Supplementation of depth information; Stud welding; 3D vision

1 Introduction

Stud welding has been widely used in various scenarios, including nuclear power equipment [1], boiler equipment [2,3], bridge structures [4], building composite structures [5], and shipbuilding [6,7]. For example, the average consumption of studs per individual bridge amounts to 250,000 studs, and millions of studs are required for welding in the hull and compartments of ships [6]. Taking the studs on the upper flange surface of an I-beam as an example, before stud welding, workers are required to meticulously mark lines to locate studs on the surfaces of components based on Computer-Aided Design (CAD) drawings. This process is rather time-consuming, where positioning a stud typically takes around 10 seconds [8]. Moreover, workers will spend more time positioning studs on curved components, and the verticality of stud welding cannot be guaranteed.

During the process of positioning and welding studs, workers are required to maintain a prolonged and extremely forward-bent posture [9]. According to [10], when the duration of this bending posture exceeds four hours, the risk of experiencing lower back pain is heightened. The daily working hours for welding workers would commonly exceed four hours.

In the current industry, the manufacturing process of steel beams has been highly automated in terms of steel plate cutting and welding. However, the welding of studs on the surfaces of components is still manually performed, which decreases the efficiency of the whole production line.

To increase the efficiency of stud welding, a robotic welding framework was proposed in this paper that involves a robot arm, a structured light camera, and a 2D drawing. In particular, a Fast-Pixel-Matching (FPM) algorithm was developed to convert the welding position from 2D drawings to 3D working space.

2 Related Work

With the evolution of CAD technology, abundant manufacturing information is embedded within drawings.

Taking computer numerical control (CNC) machine tools as an example, manufacturing 2D components often requires only a 2D Drawing Exchange Format (DXF) file, as seen in the case of CNC engraving machines [11]. However, if drilling is to be performed on curved surfaces, a 3D SolidWorks model becomes necessary [12]. This approach is viable in the field of mechanical engineering, where engineers commonly utilize 3D software for design. However, civil engineers tend to be accustomed to 2D design [13] and most of the structural designs were still represented using 2D drawings [14,15].

For example, existing automated stud welding equipment typically requires only 2D DXF drawings for 2D components [1]. During the shear stud welding process, the robotic arm descends automatically with its end-effector pointing vertically downward. The force sensor at the robotic arm's end-effector detects contact between the welding gun and the steel plate, triggering

the welding signal for the welding operation.

However, when dealing with curved components, due to the requirement of perpendicular installation of shear studs to the steel plate surface, the robotic arm's end-effector needs to maintain a perpendicular orientation at the welding point relative to the steel plate surface. Therefore, when dealing with 3D components, existing method requires the establishment of a 3D model based on 2D drawings to provide Cartesian coordinates and orientation information for shear stud welding[8], which proves to be quite time-consuming [16]. Hence, existing automated stud welding equipment does not align with the design conventions in civil engineering.

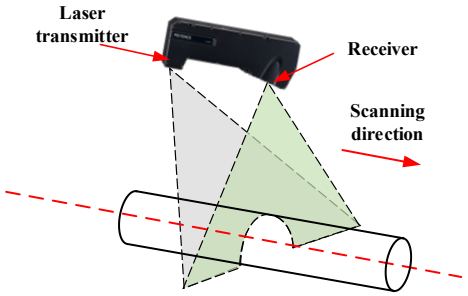

(a) Light section sensor

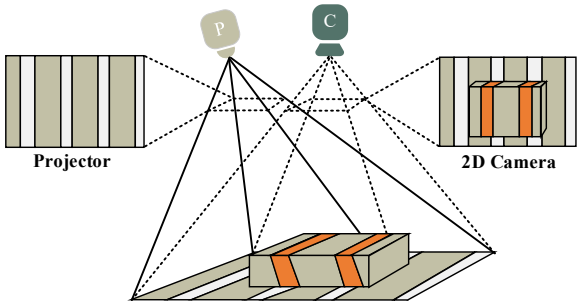

(b) Structured light camera

Figure 1. The method of point cloud data acquisition

In general, 2D drawings only contain planar coordinate information, thus necessitating the use of sensors to supplement missing Z-axis coordinates and orientation information of the target, such as studs. To acquire the missing information, in [2,3], the authors presented a measurement method that integrated 2D drawings with a light section sensor for the pose of the stud. The light section sensor captures point cloud data in the vicinity of the points to be welded, enabling the fitting of the orientation directional vector of the shear studs. However, the cost of the light section sensor is generally higher than that of a structured light camera. As illustrated in Figure 1(a), this method requires controlling the movement of the light section sensor in a specific direction to obtain point cloud data. In contrast, the structured light camera shown in Figure 1(b) can capture point cloud data within an area with a simple overhead shot. Hence, using a structured light camera to supplement missing 3D coordinate information in 2D drawings would result in higher operational efficiency.

In the literature, 3D cameras have been used in several fields, such as fruit recognition [17], trajectory tracking [18], and pose tracking [19,20]. In most of these applications, the pixel coordinates $[u,v]^T$ and corresponding depth information z_{cam} can be directly obtained using the object detection algorithm and 3D camera, which enables the calculation of the object's world coordinates $[x_w, y_w, z_w]^T$ using Equation (1) (for robotic operation, such as picking a fruit).

$$\begin{bmatrix} x_w \\ y_w \\ z_w \\ 1 \end{bmatrix} = z_{cam} \begin{bmatrix} R & T \\ 0 & 1 \end{bmatrix} \begin{bmatrix} f_x & 0 & p_x \\ 0 & f_y & p_y \\ 0 & 0 & 1 \end{bmatrix}^{-1} \begin{bmatrix} u \\ v \\ 1 \end{bmatrix} \quad (1)$$

In the stud welding setting, however, the goal is to find the pixel coordinates, i.e., the welding point in the image, that corresponds to the given world coordinates $[x_w, y_w]^T$ from the 2D drawings. Due to the absence of world coordinates z_w and depth information z_{cam}, the pixel coordinates $[u,v]^T$ (guiding robotic arm) couldn't be directly determined based on $[x_w, y_w]^T$, using Equation (1).

To overcome this problem, this paper presents a new point-searching algorithm, i.e., FPM, which enables a rapid determination of corresponding pixel coordinates $[u,v]^T$ based on planar world coordinates $[x_w, y_w]^T$.

3 Method

The proposed framework comprises the following three steps.

1. The AutoCAD plug-in is developed to extract the planar world coordinates of studs and circular marks based on C# programming language and the .Net API [21].
2. Based on planar world coordinates $[x_w, y_w]^T$, FPM is proposed for a rapid search of pixel coordinates $[u,v]^T$ corresponding to planar world coordinates $[x_w, y_w]^T$, which allows for the supplementation of missing Z-axis world coordinates z_w using Equation (1).
3. Near the pixel coordinates $[u,v]^T$, select several

other pixel coordinates and their corresponding world coordinates for obtaining the orientation vector $\vec{n}$ of the stud welding position. With the 3D world coordinates $[x_w, y_w, z_w]^T$ and the orientation vector $\vec{n}$, the pose of the robotic arm end effector can be calculated.

3.1 AutoCAD Plug-in

In 2D drawings, there are typically tens of thousands of studs, and manually marking lines for positioning is a labour-intensive and highly repetitive task. Therefore, we developed an AutoCAD plug-in to extract the coordinates of studs. The primary development approach is as follows:

1. Extracting the central coordinates of circles as the coordinates for studs. (shear studs are generally represented as circles in 2D drawings.)
2. As illustrated in Figure 2, it is necessary to draw circular marks O, A, and B on the 2D drawing and establish a local frame. Hence, the coordinates of studs $[x_l, y_l]^T$ in the local frame can be extracted.
3. Transforming the coordinates $[x_l, y_l]^T$ of studs in the local frame to the world frame, as detailed in Section 3.1.1.

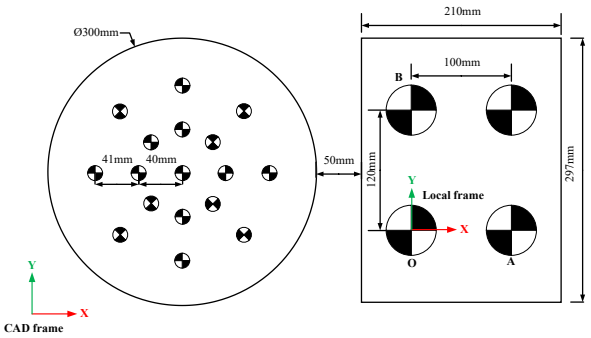

Figure 2. CAD drawing

A demo showing the extraction results of studs in 2D drawings can be found at: https://youtu.be/nrdaXvO8dkE.

3.1.1 Transformation of Planar Coordinates

The planar coordinates of studs require converting from the local frame to the world frame, and the method is as follows:

1. As shown in Figure 3, put the 3D printed component and marking board on the working plane according to their geometric relationships in the 2D drawing.
2. As shown in Figure 3, the structured light camera mounted on the end of the robotic arm captures an overhead view of the marking board, obtaining RGB and depth images. Utilizing the Hough transform method [22], the pixel coordinates of the center points of circular marks O, A, and B are acquired. With Equation (1), the coordinates of the centers of circular marks O, A, and B in the world frame can be calculated.

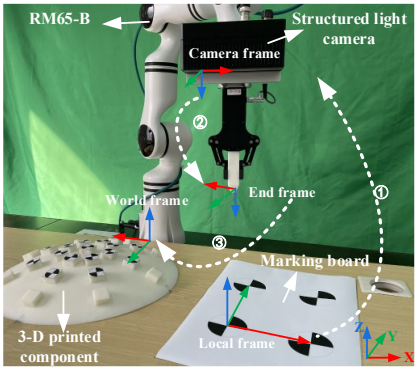

Figure 3. Experimental setup and the transformation between different frames

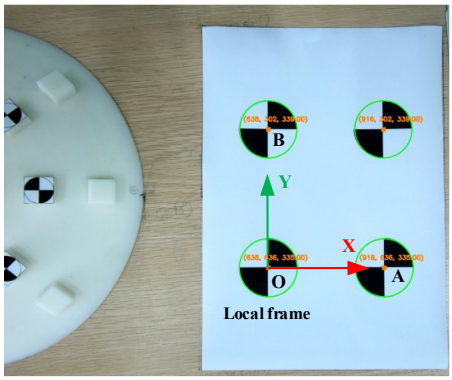

Figure 4. The center of circle recognition results using the Hough transform method

3. The center of circle recognition results $[u, v, z_{cam}]^T$ using the Hough transform method are shown in Figure 4, and substitute $[u, v, z_{cam}]^T$ into Equation (1) to obtain the world coordinates of marks O: $[x_w^O, y_w^O]^T$, A: $[x_w^A, y_w^A]^T$, B: $[x_w^B, y_w^B]^T$. Having obtained the coordinates of marks in the world frame, utilizing Equation (2) allows for the transformation of the coordinates of studs from the local frame to the world frame.

$$\begin{bmatrix} x_w \\ y_w \\ 1 \end{bmatrix} = M_{local2world} \begin{bmatrix} x_l \\ y_l \\ 1 \end{bmatrix} \quad (2)$$

Where $M_{local2world}$ is the transformation matrix from local frame to world frame, and its expression is as follows:

$$M_{local2world} = \begin{bmatrix} \cos < \overrightarrow{OA}, \overrightarrow{X} > & \cos < \overrightarrow{OB}, \overrightarrow{X} > & x_w^O \\ \cos < \overrightarrow{OA}, \overrightarrow{Y} > & \cos < \overrightarrow{OB}, \overrightarrow{Y} > & y_w^O \\ 0 & 0 & 1 \end{bmatrix} \quad (3)$$

Where $\overrightarrow{X} = [1,0]^T$, $\overrightarrow{Y} = [0,1]^T$.

3.2 Fast Pixel-Matching Process

After completing the coordinates transformation in Section 3.1.1, one can use the planar world coordinates of the studs to control the movement of the robot-mounted structured light camera, positioning above the 3D printed component, as shown in **Error! Reference source not found.**. This enables the acquisition of RGB and depth images of the target area.

When transforming the coordinates of studs from the local frame to the world frame, with only knowledge of the planar world coordinates $[x_w, y_w]^T$, it is not possible to calculate the corresponding pixel coordinate $[u,v]^T$ using Equation (1).

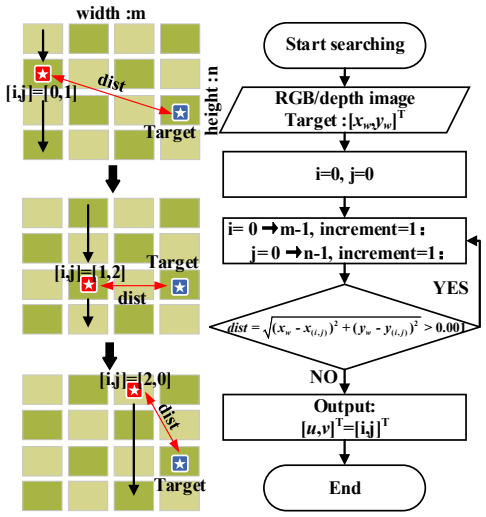

Figure 5. Iterative search process of BFS

However, it is feasible to adopt BFS for calculating each pixel coordinate corresponding to the world coordinate in the image. In Figure 5, the pixel coordinates currently being searched are $[i,j]^T$, and their corresponding planar world coordinates in the plane can be calculated by Equation (1) as $[x_{(i,j)}, y_{(i,j)}]^T$.

By comparing $[x_{(i,j)}, y_{(i,j)}]^T$ with $[x_w, y_w]^T$, when the 'dist' ($dist = \sqrt{(x_w - x_{(i,j)})^2 + (y_w - y_{(i,j)})^2}$) between the currently searched pixel (red start) and with target pixel (blue start) is less than 0.001m, the currently searched pixel coordinate $[i,j]^T$ can be considered as the pixel coordinate $[u,v]^T$ for the welding point of the stud.

However, it should be noted that BFS is quite time-consuming, and we proposed another fast point searching method, FPM, with details outlined below.

3.2.1 Algorithm Design

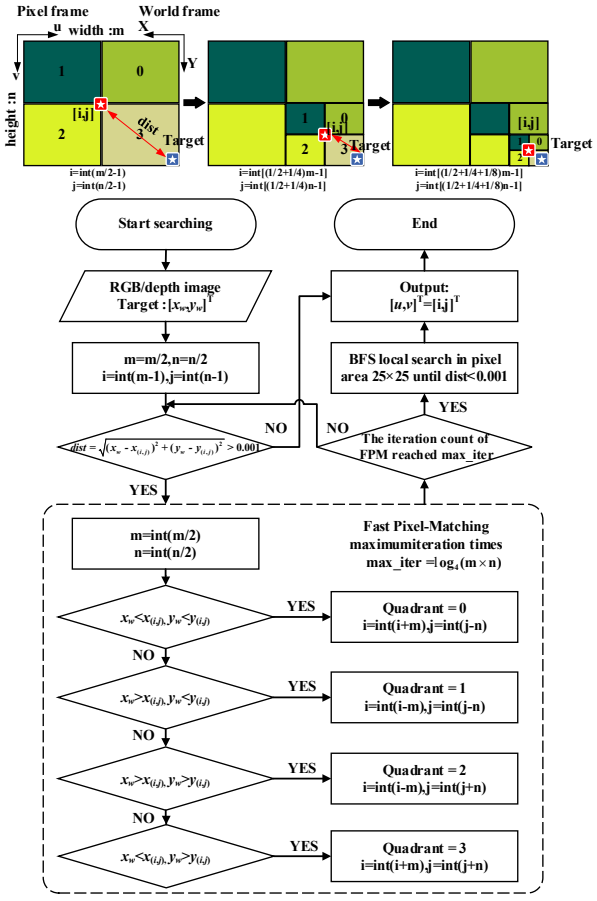

Figure 6. Iterative search process of the FPM process

It is important to note that, for the FPM application, as illustrated in Figure 6, the image pixel frame has its u-axis opposite to the X-axis of the world frame, while the v-axis aligns with the Y-axis of the world frame, dividing the image into four quadrants labeled 0, 1, 2, and 3.

Based on the above assumptions, Figure 6 illustrates the first three iterations of the algorithm's search process, and the computational iterative process of the algorithm is as follows.

As illustrated in Figure 6, when employing FPM for the search, during the first round of iteration, the world coordinate $[x_{(i,j)}, y_{(i,j)}]^T$ corresponding to the currently searched pixel coordinate $[i, j]^T$ at the center of the image is calculated. The coordinate $[x_{(i,j)}, y_{(i,j)}]^T$ is then compared with $[x_w, y_w]^T$, determining the next search quadrant based on the principle from Equation (3) to Equation (6). Through repeated cycles until 'dist' is less than 0.001m, the pixel coordinate $[u, v]^T$ corresponding to the planar world coordinate $[x_w, y_w]^T$ can be rapidly matched.

$$x_w < x_{(i,j)}, y_w < y_{(i,j)}, Quadrant = 0 \quad (3)$$

$$x_w > x_{(i,j)}, y_w < y_{(i,j)}, Quadrant = 1 \quad (4)$$

$$x_w > x_{(i,j)}, y_w > y_{(i,j)}, Quadrant = 2 \quad (5)$$

$$x_w < x_{(i,j)}, y_w > y_{(i,j)}, Quadrant = 3 \quad (6)$$

The space complexity of FPM is $O(\log_4 m \times n)$. For an image resolution of 1280 × 960, the correspondence between $[x_w, y_w]^T$ and $[u, v]^T$ can be determined with a maximum of 11 ($\log_4 1280 \times 960 \approx 11$) iterations.

After 11 iterations of FPM, BFS is applied within a pixel range of 25 × 25 to obtain pixel coordinates, and 'dist' can converge to 0.001m. The camera's field of view and resolution are respectively 460mm × 360mm and 1280 × 960, so approximately 3 pixels correspond to each millimeter. Therefore, a pixel range of 25 × 25 (±4 mm range) is considered appropriate.

For the sake of convenience in expression, the combined process of FPM and BFS will be referred to as the FPM process in the following content.

In theory, only 11+25 × 25 = 636 iterations are needed in the FPM process to accomplish the process. However, using only the BFS method would require iterations of 1280 × 960 = 1,228,800, which is almost 2000 times higher than that of the FPM method.

4 Experimental Setup and Results

4.1 Experimental Setup

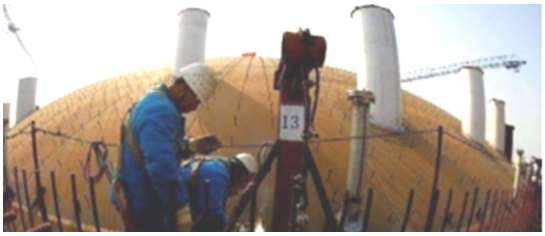

Figure 7. The dome of the LNG storage tank [23]

As shown in **Error! Reference source not found.**, the experimental setup is composed of a robotic arm (RM-65), structured light camera (PS800-E1, resolution 1280 × 960), 3D printed component, and a marking board. The prototype of the 3D printed component is shown in Figure 7, which is the steel structural dome at the top of the LNG storage tank. An experiment was conducted to assess the efficiency and accuracy of the FPM process.

In the experiment, a total of 17 welding points shown in **Error! Reference source not found.**(a) were considered as the target for point searching. for precision comparison, in this paper, the ground truth of the depth information of these welding points was obtained by using the mouse to click on the pixel coordinates at the center of each mark in **Error! Reference source not found.**(a), and then transforming them into world coordinates using Equation (1).

4.2 Experimental Results

4.2.1 Efficiency

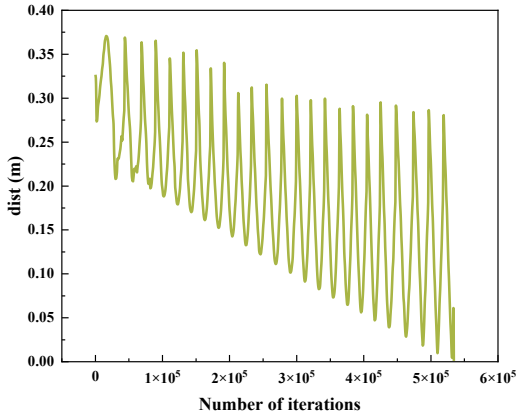

(a) BFS

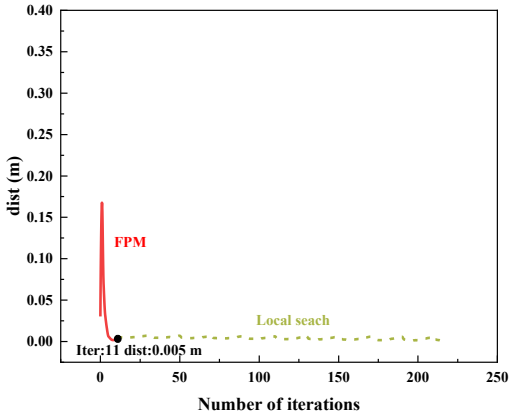

(b) FPM process

Figure 8. The number of iterations for the pixel search in the BFS and FPM process

Based on the comparison shown in Figure 8, FPM achieved a much faster convergence than that of BFS. In particular, a total of 217 iterations were performed in the FPM process, while only BFS required 534,115 iterations, the comparative data can be found in Table 1.

The efficiency of the FPM process, BFS, and the manual method is detailed in Table 2 for comparison. FPM exhibits exponential convergence, with an iteration efficiency 47,604 times greater than BFS. In Table 2, the time required for manual positioning was calculated based on the assumption that locating a welding point would require 10 seconds by marking lines [8].

In terms of iteration time, the efficiency of the FPM process is 21 times that of BFS and 105 times that of manual methods, allowing for the rapid determination of pixel coordinates corresponding to planar world coordinates.

Table 1. Comparison of Iteration Steps between the FPM process and BFS

Method	FPM process	BFS
dist < 0.001m	217	534,115

Table 2. The time required for positioning using different methods

Method	Time (s)	Efficiency ratio
FPM process	1.62	105
BFS	34.4	5
Manual method	170.0	1

4.2.2 Accuracy

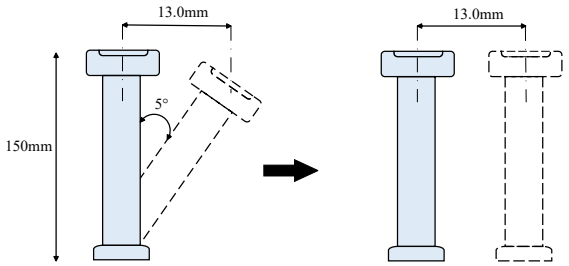

Figure 9. Conversion from verticality to offset

As shown in Figure 9, the ‘Code for acceptance of construction quality of steel structures’ only has a clear requirement for the verticality of studs. The inclination angle should not exceed 5 degrees [24]. Taking the commonly used size of stud M16 × 150 as an example, the maximum offset at the top of the stud can be calculated as 13.0mm. This calculation is used to determine the maximum allowable offset in the plane of the stud.

The positioning accuracy errors of the FPM process and BFS compared with the manual method, as shown in Figure 10, indicated that they fully meet the code requirement, and the maximum error was only 2.09 mm in the direction of Z axis.

Figure 11 presents the results of the 17-pixel coordinates mapped to the RGB image obtained through the FPM process. The green points represent the pixel coordinates corresponding to the planar world coordinates.

Additionally, comparing with related literature on x-y positioning accuracy, in [7], the proposed method has a maximum error of 8mm, while the FPM process has a maximum error of 7.1mm, representing a 9% improvement in accuracy. However, this approach relies on the manual use of an IMU device to designate the position of the welding points, while the method proposed in this paper can automatically search for the pixel coordinates of welding points without manual guidance.

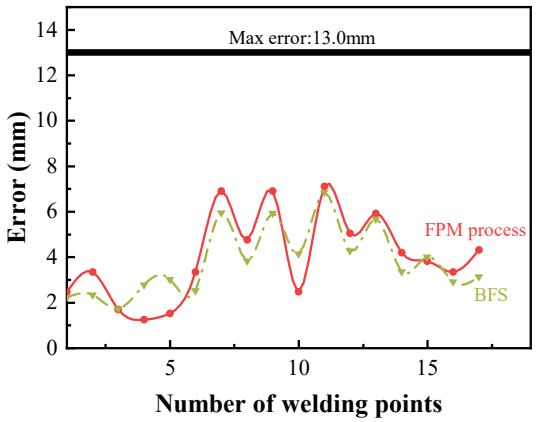

Figure 10. The x-y positioning accuracy errors of FPM process and BFS compared with the manual method

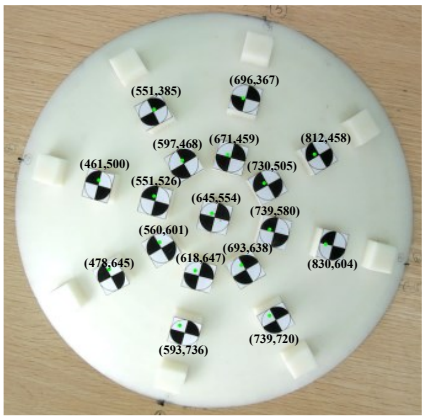

Figure 11. Pixel Coordinate Mapping by FPM process

4.2.3 Analysis of Experimental Results

This section conducts an analysis of the efficiency and errors in the iterative process of FPM process.

Efficiency:

As shown in Figure 8(b), the efficiency of FPM process is affected by the iterations of local search. Based on our experiments, the local search process can be significantly shortened or even avoided when the quality of the depth map is improved by using better cameras with higher accuracy in calculating the depth data.

The quality of the depth map is influenced by various factors, including but not limited to oversaturation caused by ambient light [25], interference from external active illumination source [26,27], and so forth. Therefore, missing depth (holes) are always observed in the depth map.

For the issue of missing depth, the following method is employed: the depth equivalent value for the currently searched pixel with missing depth is determined by calculating the average depth of non-zero points within a 7×7 pixel range centered on it.

The depth values for pixels with missing depth information are approximations, leading to errors when calculating world coordinates using Equation 1. And given that the maximum search iterations for FPM are set at $\log_4 1280 \times 960 \approx 11$ times, it becomes challenging to converge to values below 1mm, especially in cases of poor depth map quality. Hence, local search process is necessary for further refinement under such circumstances.

Therefore, the efficiency can be significantly improved by using better structured light camera with relatively fewer missing depth.

Positioning accuracy:

In our experiment, the errors in positioning mainly stem from three aspects that should be considered in further studies:

1. The quality of the depth map obtained from the structured light camera.
2. The accuracy of hand-eye calibration.
3. The relative positional relationship between the marking board and 3D printed components placed on the actual working table versus that plotted in the 2D drawings.

5 Conclusion and Future Research

To increase the efficiency of shear stud welding on the surface of 3D objects, a robotic manufacturing framework was proposed in this paper, which included a robotic arm, a structured light camera, and a 2D drawing. In particular, a fast point-searching algorithm, FPM, was developed and validated against a point-positioning experiment in our lab.

Based on our experiment, the efficiency of the FPM process is found to be 20 times higher than the traditional BFS method, and 100 times higher than the manual positioning through marking lines, and its positioning accuracy meets the code requirements.

Future research can be conducted to improve the proposed framework in the following aspects:

1. Based on the obtained world coordinates and the orientation vector at the welding point, the pose of the robotic arm's end-effector can be further calculated to accomplish the welding and evaluate its quality.
2. In the current setting, the robotic arm is fixed on the working plane. A more flexible welding platform can be developed by mounting the robotic arm on the linear axis or deploying it on an Unmanned Ground Vehicle (UGV) to accomplish the welding task on construction sites.

6 Acknowledgment

This research was supported by the National Natural Science Foundation of China (Grant No. 52278177, 52108136, and 52308312) and the National Key Research and Development Program of China (No. 2023YFC3806804).

References

[1] Hongqi Jiang, Kang Du, Wen Sun, Guangchao Wang, Aining Jiang. The Design of a Large Automatic Welding Equipment for Shear Studs. *Machine Design and Research,* 36(05): 208-215, 2020.

[2] Xudong Ji, Youdong Chen, Song Yang. Stud welding system using an industrial robot for membrane walls. *The International Journal of Advanced Manufacturing Technology,* 121(11-12): 8467-8477, 2022.

[3] Youdong Chen, Qi Hu. Dual-robot stud welding system for membrane wall. *Industrial Robot: the international journal of robotics research,* 49(1): 132-140, 2022.

[4] Alexander H Slocum, Andrew G Ziegler. An automated shear stud welding system. *Robotics autonomous systems,* 6(4): 367-382, 1990.

[5] Andrew Glenn Ziegler. The design and fabrication of an automated shear stud welding system, Massachusetts Institute of Technology, 1988.

[6] Rasmus S Andersen, Simon Bøgh, Thomas B Moeslund, Ole Madsen. Intuitive task programming of stud welding robots for ship construction. *2015 IEEE International Conference on Industrial Technology (ICIT)*, pages 3302-3307, 2015.

[7] Rasmus S Andersen, Simon Bøgh, Thomas B Moeslund, Ole Madsen. Task space HRI for cooperative mobile robots in fit-out operations inside ship superstructures. *2016 25th IEEE International Symposium on Robot and Human Interactive Communication (RO-MAN)*, pages 880-887, 2016.

[8] Futao Diao. A new type of automatic shear studs welding workstation suitable for curved panels with dual welding guns. (*patent, in Chinese*)

[9] Nathan B Fethke, Lauren C Gant, Fred Gerr. Comparison of biomechanical loading during use of conventional stud welding equipment and an alternate system. *Applied ergonomics,* 42(5): 725-734, 2011.

[10] EB Holmström, J Lindell, U Moritz. Low back and neck/shoulder pain in construction workers: occupational workload and psychosocial risk factors. Part 2: Relationship to neck and shoulder pain. *Spine,* 17(6): 672-677, 1992.

[11] Huibin Yang, Juan Yan, Automation. DXF file identification with C# for CNC engraving machine system. *Intelligent Control,* 6(01): 20-28, 2015.

[12] Anastasios Tzotzis, Athanasios Manavis, Nikolaos Efkolidis, Panagiotis Kyratsis. CAD-BASED AUTOMATED G-CODE GENERATION FOR DRILLING OPERATIONS. *International Journal of Modern Manufacturing Technologies,* 13 177-184, 2021.

[13] Lucas Francisco Martins, Marcio Augusto Reolon Schmidt, André Luiz de Alencar Mendonça. Graphical representation analysis of complementary civil projects using" cad 2d"," bim" and" ra" and identification of interferences. *Boletim de Ciências Geodésicas,* 25, 2019.

[14] Mohsen Foroughi Sabzevar, Masoud Gheisari, L James Lo. Improving access to design information of paper-based floor plans using augmented reality. *International Journal of Construction Education Research,* 17(2): 178-198, 2021.

[15] Robert Eadie, Mike Browne, Henry Odeyinka, Clare Mckeown, Sean Mcniff. BIM implementation throughout the UK construction project lifecycle: An analysis. *Automation in construction,* 36 145-151, 2013.

[16] Bin Yang, Boda Liu, Dayu Zhu, Binghan Zhang, Zhichen Wang, Ke Lei. Semiautomatic structural BIM-model generation methodology using CAD construction drawings. *Journal of Computing in Civil Engineering,* 34(3): 04020006, 2020.

[17] Hanwen Kang, Hongyu Zhou, Xing Wang, Chao Chen. Real-time fruit recognition and grasping estimation for robotic apple harvesting. *Sensors,* 20(19): 56-70, 2020.

[18] Andrea Carron, Elena Arcari, Martin Wermelinger, Lukas Hewing, Marco Hutter, Melanie N Zeilinger, Automation Letters. Data-driven model predictive control for trajectory tracking with a robotic arm. *IEEE Robotics,* 4(4): 3758-3765, 2019.

[19] Bowen Wen, Chaitanya Mitash, Baozhang Ren, Kostas E Bekris. se (3)-tracknet: Data-driven 6d pose tracking by calibrating image residuals in synthetic domains. *2020 IEEE/RSJ International Conference on Intelligent Robots and Systems (IROS)*, pages 10367-10373, 2020.

[20] Sulabh Kumra, Shirin Joshi, Ferat Sahin. Antipodal robotic grasping using generative residual convolutional neural network. *2020 IEEE/RSJ International Conference on Intelligent Robots and Systems (IROS)*, pages 9626-9633, 2020.

[21] Li Zhang, Peng Zhang. CAD secondary development technology based on. NET API. *IOP Conference Series: Materials Science and Engineering*, p. 072052, 2020.

[22] HK Yuen, John Princen, John Illingworth, Josef Kittler. Comparative study of Hough transform methods for circle finding. *Image vision computing,* 8(1): 71-77, 1990.

[23] SLS Bearings.The product catalog of shear studs. O n-line: https://www.slsbearings.com/slsbnn/files/SLS%20BNN_Shear%20Stud%20catalogue%20%202020.pdf, Accessed: 22/11/2023.

[24] GB 50205-2020, Code for acceptance of construction quality of steel structures, China Planning Press Beijing, China, 2020.

[25] R. A. El-Laithy, J. Huang, M. Yeh. Study on the use of Microsoft Kinect for robotics applications. *Proceedings of the 2012 IEEE/ION Position, Location and Navigation Symposium*, pages 1280-1288, 2012.

[26] Kai Berger, Kai Ruhl, Yannic Schroeder, Christian Bruemmer, Alexander Scholz, Marcus A Magnor. Markerless motion capture using multiple color-depth sensors. *VMV*, pages 317-324, 2011.

[27] D Alex Butler, Shahram Izadi, Otmar Hilliges, David Molyneaux, Steve Hodges, David Kim. Shake'n'sense: reducing interference for overlapping structured light depth cameras. *Proceedings of the SIGCHI Conference on Human Factors in Computing Systems*, pages 1933-1936, 2012.